Monitoring of the 2011 March 11 Off-Tohoku 9.0 Earthquake with Super-Tsunami Disaster by Implementing fully polarimetric high resolution POLSAR Techniques

Gulab Singh, *Member, IEEE,* Yoshio Yamaguchi, *Fellow, IEEE* ,Wolfgang-Martin Boerner, *Life Fellow, IEEE,* Sang-Eun Park, *Member, IEEE*

***Abstract*—This paper reflects the polarimetric synthetic aperture radar (POLSAR) data utilization for near-real time earthquake and/or tsunami damage assessment in urban areas. In order to show the potential of the fully polarimetric high resolution polarimetric SAR (POLSAR) image data sets, a four-component scattering power decomposition scheme has been developed and applied to monitor near-real time earthquake and tsunami disaster damages. The test site for natural disaster damages has been selected parts of the coastal area affected by the March 11, 2011 9.0 magnitude earthquake that struck off Japan's northeastern coast and triggered a super- tsunami. The color-coded images of the scattering power decomposition scheme are simple and straightforward tool to interpret the changes over the earthquake/tsunami affected urban areas and man-made infrastructures. This method also holds other types of natural (typhoon or tornado) and manmade disaster assessments application. It is found that the double bounce scattering power is the most promising of the input parameters to detect automated disaster affected urban areas at pixel level. It is also observed that the very high resolution POLSAR images are required for superior urban area monitoring over the oriented urban blocks with respect to the illumination of radar.**

***Index Terms*—radar polarimetry, scattering power decomposition, polarimetric synthetic aperture radar, high resolution remote sensing, tsunami & earthquake disaster assessment, Off-Tohoku, Japan.**

I. Introduction

IN RECENT decades, earthquake and tsunami hazards have frequently occurred causing significant loss of life and devastating damage to property and infrastructure [1]. It is quite difficult to obtain an immediate response of large-scale earthquakes and tsunami disaster areas by ground survey based methods [2]. The ground survey method is accurate but highly time consuming and manpower extensive, which causes delays in assessment responses to rescue teams. Since these kind of natural disasters will continue to occur, observations by air-borne, high-altitude unmanned vehicle or space-borne high resolution sensor techniques are needed to shorten the time lag of ground survey based damage assessment at large scales [3] in order to properly and swiftly provide localized destruction assessments to rescue agencies regarding earthquake/tsunami affected areas for rescue operations. Since microwave radar remote sensing is a suitable tool for monitoring the near-real time earthquake and tsunami damage at large scales, at anytime of day or night, its implementation becomes of vital relevance to governmental and other agencies for initiating swift and well orchestrated rescue operations. Hitherto, several methods are available to monitor earthquake and tsunami damages by using multispectral and monochromatic optical images as well as mono/dual-polarization SAR images [4]-[6]. High resolution multispectral optical images enable direct visual interpretation of the damages and are rather straightforward and simple to interpret by users. However, optical remote sensing fails under cloudy, foggy and hazy as well as severe rainy conditions for monitoring near-real time damage. Single wavelength SAR images obtained from fixed single and/or dual polarization sensors are independent of meteorological conditions, but are difficult to interpret and require tedious computational analyses for at most incomplete assessments only.

The aim of this paper is to generate information from high resolution polarimetric SAR images to identify directly the differences or damages between pre- and post-tsunami conditions of the affected regions. However, single observations using conventional SAR images makes it difficult to generate desirable images ready for direct visual interpretation. In case we are given multi-wavelength mono/dual-polarization SAR image data sets, it could possibly be done similar to cloud free multi/hyper-spectral optical

Manuscript received June 27, 2012; revised October 26, 2012; accepted November 21, 2012. This work was supported in part by the Ministry of Education, Japan under the Space Sensing Project Grant at Niigata University.

Gulab Singh, Yoshio Yamaguchi and Sang-Eun Park are with the Graduate School of Science and Technology, Niigata University, Niigata, 950-2181, Japan, (phone/fax: +81-25-262-6752 e-mail: g.singh@wave.ie.niigata-u.ac.jp; yamaguch@ie.niigata-u.ac.jp ; spark@wave.ie.niigata-u.ac.jp).

Wolfgang-Martin Boerner is with the Department of Electrical & Computer Engineering, the University of Illinois at Chicago, IL 60607-7018 USA.

imaging methods. Current space-borne SAR systems collect multiple polarization data (dual-pol or quad-pol) at a single frequency, either X- or C-band. We take the advantage of the excellent quad-polarization data sets acquired with the Japanese Advanced Land Observing Satellite-Phase Array type L-band Synthetic Aperture Radar (ALOS-PALSAR) imaging system using its high resolution POLSAR mode to produce color-coded images for monitoring earthquake and tsunami damage along the Miyagi coast affected by the March 11, 2011 tsunami. Furthermore, Very High Resolution (VHR) TerraSAR-X (X-band) and DLR-FSAR (S-band) quad polarization images were processed to prove the effect of very high resolution for extracting detailed information from the urban areas.

Paper is organized as follows. In Section II we describe the test sites and features of data sets that we have used in this study and give a brief explanation of the methods that involved in analyzing of POLSAR data. Section III presents the results. Section IV concludes the paper.

II. Test Sites, Data Used And Methods

This section discusses test sites for the monitoring of disaster area using fully polarimetric high resolution SAR data acquired with ALOS-PALSAR and for the requirements of VHR Full-POLASR images to get better information over the urban area. This section also briefly explains the recently updated the four-component scattering decomposition scheme.

A. Test Site and Data Sets for Disaster Monitoring in the Urban Area

We have selected parts of the coastal areas within the Miyagi Prefecture affected by the 11 March 2011 magnitude 9.0 Honshu, Japan earthquakes (38.322 N, 142.369 E, depth 32 km) that struck off Japan's northeastern coast and triggered a historical super-tsunami (Fig. 1). This super-tsunami, caused by the most powerful known earthquake ever to have hit Japan and one of the five most powerful earthquakes in the world, reached that more than 7.6 m height in Ishinomaki, part of the Miyagi Prefecture, and maximum height 40.5 m was noticed in Miyako in Iwate Prefecture. A Japanese National Police Agency report [7] on Sept. 10, 2012 confirmed 15,870 deaths, 6,114 injured and 2,814 people missing across twenty prefectures of Japan. Out of these numbers, 9,527 deaths, 4,140 injured and 1,394 people missing are reported within Miyagi prefecture. Moreover, the earthquake and tsunami caused extensive and severe structural damage in North-Eastern Japan, including heavy damage to buildings, roads and railways as well as fires in many areas, and a dam collapse. According to National Police Agency of Japan report on Sept.10, 2012, more than 237,030 buildings were collapsed and 224,225 were partially damaged in Miyagi prefecture by the earthquake/tsunami [7]. The information about the collapsed buildings and tsunami covered areas over the off-Tohoku region by tsunami disaster also mapped by the Association of Japanese Geographers, and Geospatial Information, Authority of Japan [8].

In order to examine the capability of quad-polarization SAR image data-sets for monitoring damages, we used the ALOS-PALSAR fully polarimetric, single look complex (SLC), level 1.1(ascending orbit) images acquired over study areas before (April 02, 2009 and November 21, 2010) and after the earthquake/tsunami (April 8, 2011) struck (Table I).

During the April, 2009 acquisition, most of the agricultural areas were prepared for rice transplantation. In the November, 2010 image, agricultural fields were harvested and paddy fields were bare. After the disaster acquisition in April, 2011, the agricultural fields were affected by tsunami flow. The affected areas due to the earthquake/tsunami disaster were confirmed by using the ground-truth information provided by the Association of Japanese Geographers, and Geospatial Information, Authority of Japan [8], which is illustrated in Fig. 2. In addition, four patches (A-D) are selected for exploring the changes in the study area by earthquake/tsunami disaster. The patch A is selected over the vegetated area, the patch B is taken in the agricultural area, the patch C is chosen in the urban areas of Ishinomaki city, and the patch D is preferred over the Onagawa urban region/Onagawa Bay. The changes over the patch A occurred mainly due to the damages of trees and deposition mud by tsunami flow forces. The changes over patch B are due to the deposition of collapsed and washed out house debris and water cover over the bare agriculture field area by tsunami flow. The changes over patches C and D occurred by washout and the damage of building blocks after the earthquake/tsunami disaster. The changes in these patches (A-D) were also cross checked with before (April 04, 2010 and June 26, 2010) and after (April 06, 2011) the disaster ultra high resolution Google earth optical images.

B. Test Sites and Data Sets for Proving the Requirement of VHR POLSAR Images over Urban Area

Due to non-availability of VHR Full-POLSAR images before and after the earthquake/tsunami disaster over the Ishinomaki, Miyagi Prefecture, three more data sets were acquired to show the requirements of the VHR Full-POLSAR images over the highly oriented urban areas in other part of the earth. Out of these three images, two images [one image from high resolution fully polarimetric ALOS-PALSAR products during the descending orbits in the form of SLC, level 1.1 products, and a second image from the experimental mode for VHR fully polarimetric TerraSAR-X products during the descending orbits in the form of single look slant range complex (SSC) product] were acquired by spaceborne POLSAR sensor over the Niigata city and environments, Japan (see Table I) and another one VHR POLSAR SLC image was acquired from the DLR airborne F-SAR S-band system over the Kaufbeuren, Germany. Although, these data sets are acquired over the different region but these data can serve the purpose that the improvements to be found by using VHR POLSAR image.

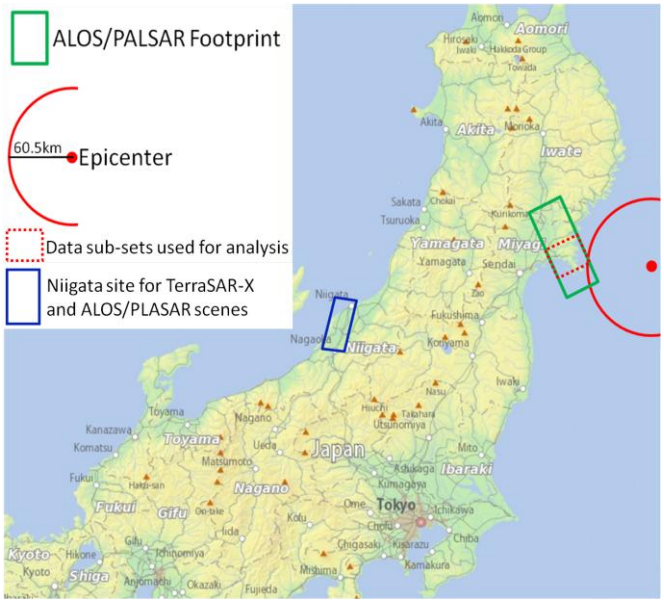

Fig.1. Location map of selected disaster affected site near Ishinomaki, Miyagi Prefecture and of selected test site over Niigata for proving the requirement of VHR Full-POLASR image to get better information over the urban area

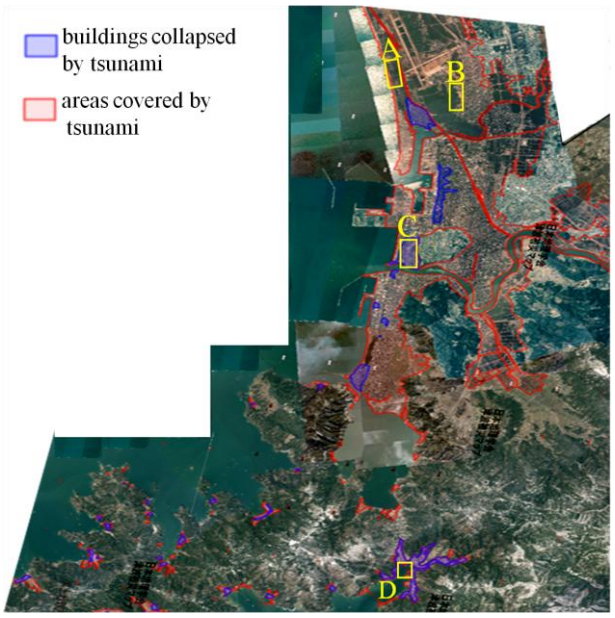

Fig. 2. The ground truth data. The patch A shows the vegetation area on relatively flat surface area, the patch B represents the agricultural area over relatively flat ground, the patch C illustrate the urban areas of Ishinomaki city, and the patch D demonstrates the Onagawa urban region/Onagawa Bay.

Table I. Characteristics of the quad polarization spaceborne ALOS-PALSAR SLC data sets and TerraSAR-X SSC data and an airborne F-SAR SLC quad polarization data

Date	Sensor	Frequency (GHz)	Off-nadir angle (^{0})	Resolution (m)	Region	Main purpose to use data sets
20090402	PALSAR	1.27	21.5	30	Ishinomaki	To monitor temporal and post disaster effects in the urban areas
20101121	PALSAR	1.27	21.5	30	Ishinomaki	
20110408	PALSAR	1.27	21.5	30	Ishinomaki	
20100304	PALSAR	1.27	21.5	30	Niigata	To show the strength and efficacy of VHR in the urban area
20100422	TerraSAR-X	9.6	36.7	2	Niigata	
20100608	DLR F-SAR	3.25	37.0	0.5	Kaufbeuren, Germany	

C. *Methods: Utilization of Full-POLSAR Model Based Decomposition*

For this investigation all POLSAR data are acquired from the monostatic POLSAR sensor configuration. In this case, the scattering matrix carries useful information by five independent quantifies (three amplitudes and two phase differences) [9], [10]. Various methods have been proposed in the last century to decompose the scattering matrix [11], [12] for characterizing the point targets. On the other hand, the complete scattering information in the form of second order statistics like coherency or covariance matrix is required to characterize the distributed targets [11], [13] - [16]. There exist 9 independent polarization parameters in the coherency matrix [*T*] as the second order statistics [17] - [20]. The coherency matrix [*T*] is defined as

$$[T]=\begin{bmatrix} T_{11} & T_{12} & T_{13} \\ T_{21} & T_{22} & T_{23} \\ T_{31} & T_{32} & T_{33} \end{bmatrix}$$

$$=\frac{1}{2}\begin{bmatrix} \left\langle |S_{HH}+S_{VV}|^2 \right\rangle & \left\langle (S_{HH}+S_{VV})(S_{HH}-S_{VV})^* \right\rangle & 2\left\langle (S_{HH}+S_{VV})S_{HV}^* \right\rangle \\ \left\langle (S_{HH}-S_{VV})(S_{HH}+S_{VV})^* \right\rangle & \left\langle |S_{HH}-S_{VV}|^2 \right\rangle & 2\left\langle (S_{HH}-S_{VV})S_{HV}^* \right\rangle \\ 2\left\langle S_{HV}(S_{HH}+S_{VV})^* \right\rangle & 2\left\langle S_{hv}(S_{HH}-S_{VV})^* \right\rangle & 4\left\langle |S_{HV}|^2 \right\rangle \end{bmatrix} \quad (1)$$

In (1), S_{HH}, S_{VV} and S_{HV} are the elements POLSAR scattering matrix measurements. The elements S_{HH} and S_{VV} represent the return power in co-polarized channels and the element S_{HV} corresponds to the return power in cross-polarized channel.

We have used the most recent 4-component scattering power decomposition method [21]-[22] to examine the disaster area. This decomposition scheme describes the total scattering power into surface scattering power P_s, double bounce

scattering power P_d, volume scattering power P_v, from dipole and/or oriented dihedral and helix P_c, as shown in Fig.3. This recently developed four-component scattering power decomposition scheme [21], [22] also includes the complete fully polarimetric phase information and the extended volume scattering model for oriented dihedral structures (which are most desired in the urban area [19] – [20] to estimate the appropriate volume scattering as compared to three-component decomposition [14]).

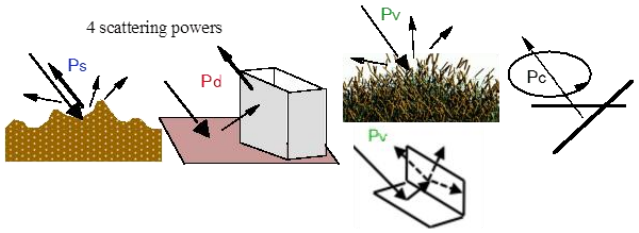

Fig.3. Illustrative examples for four-component scattering powers : surface scattering power *Ps*, double bounce scattering power *Pd*, volume scattering power *Pv* and helix scattering power *Pc*

The physical understanding of polarimetric four-component scattering mechanisms is briefly explained as follows:

1) *Surface scattering*: the scattering which takes place only on the border surface between two different but homogeneous media, from one of which radar pulse is incident on to the other [23]. The surface scattering mechanism is mainly caused by rough surfaces such as bare soil, water surface, sea surfaces, agricultural fields, etc. [14]-[16], [23] – [27].In this case, the phase difference of co-polarized components *HH-VV* is closer to zero [28], however the *HH* and *VV* magnitudes may differ. Scattering of POLSAR on the ground surface increases according to the increase of relative dielectric constant, and the direction of scattering depends on the surface roughness and the orientation of the surface [13], [29].

2) *Double bounce scattering:* This type of scattering comes from two surfaces at right angle, for example one flat on the ground (horizontal), the other upright (vertical) such as road surfaces and building walls, river surfaces and bridge structures, etc.[13] - [16]. Return single of radar hits both surfaces one after the other, and the total angle of radar reflection is π, in the backscatter direction. This double bounce scattering phenomena generates the compound scattering matrix from two surfaces and the most important consequence of this compound matrix is that the co-polarized components *HH* and *VV* are out of phase [13], [24], [28]. Typically, urban areas show double bounce scattering dominance due to the wall-ground or ground-wall interactions of the radar signal. Double bounce scattering can also occur frequently in nature, whenever there are upright vegetation stems (stalks, trunks) and a relatively smooth (and flat) surface underneath. Examples are flooded forests, and parallel (to the azimuth direction of radar) rows of rice fields, of corn fields, etc..

3) *Volume scattering:* Volume scattering can be observed if SAR beam penetrates into a medium [25]. Scattering from trees or branches, crops, subsurface, oriented buildings from the line of sight of radar and etc. [14], [17], [18], [32] are examples of volume scattering. When the radar beam interacts with the vegetation, the random scattering process (random volume scattering over the ground) will be generated.

4) Helix scattering: The helix scattering power is essentially the same as the circular polarization power [15]. The circular polarization can be generated from a source of horizontally polarized component plus vertically polarized component with 90^0 out of phase. For example, orthogonal wires with 1/8 wavelength separation structures reflects circular polarization [33]. These sources can be seen in urban area, i.e., in man-made structures such as facets of buildings or urban area with lots of wire structure placed in orthogonal directions depending on frequency [15]-[22]. In case, the sources of the helix scattering increase over the surface, the scattering helicity will increase.

Since the four-component scattering decomposition scheme in [21] is improved version of [18] and [19], fully polarimetric high resolution ALOS-PALSAR data sets as well as very high resolution data of spaceborne fully polarimetric TerraSAR-X and the fully polarimetric DLR airborne F-SAR data sets have been analyzed based on the this recently updated version of decomposition scheme. Decomposition color composite images of PALSAR data sets were generated with multi-look factors 12 times in azimuth direction and 2 times in range direction. The color composite image of TerraSAR-X data with decomposition was made with multi-look factors 10 times in azimuth direction and 12 times in range direction and the multi-look window size for the DLR F-SAR data to produce the color composite image was chosen as 10 in the range direction and 10 in the azimuth direction.

After the decomposition of ALOS-PALSAR data over the earthquake/tsunami disaster site, the four scattering components, namely the surface scattering (P_s), the double bounce scattering (P_d), the volume scattering (P_v) and the helix scattering (P_c), components were normalized by *Total Power* (*TP*) for further analysis. The normalized scattering components are defined as

$$p_s = \frac{P_s}{TP};\ p_d = \frac{P_d}{TP};\ p_v = \frac{P_v}{TP};\ p_c = \frac{P_c}{TP} \qquad (2)$$

where p_s , p_d, p_v and p_c are the normalized scattering powers corresponding to surface , double bounce , volume and helix scattering, respectively, and

$$TP = P_s + P_d + P_v + P_c \qquad (3)$$

The mean filter with 3×3 window size is applied on these normalized scattering power components images before analyzing the images in more detail.

III. RESULTS

A. Interpretation of RGB Color-Coded Images

Three (two pre-disaster and one post-disaster) images, corresponding to the same region of recovered fully polarimetric PALSAR images for the pre- *versus* post-disaster are processed by implementing the recently developed general

4-component scattering power decomposition (4-CSPD) scheme [21]. These decomposition RGB color-coded images of 20090402, 20101121, and 20110408 are presented in Fig. 4 (a), Fig. 4 (b) and Fig. 4 (c), respectively. Fig. 5 and Fig. 6, show the enlarged parts of the pre- *versus* post-tsunami 4-CSPD color-coded images for examining the tsunami damages for the patch A (vegetated area), the patch B (agricultural area), the patch C (urban region), and the patch D (urban region/Onagawa Bay) [see Fig. 2], respectively for which color-coding RGB was chosen according to established conventions [18].

Moreover, when tsunami damages the vegetations (see patch A, Fig.5), the random scattering process (random volume scattering over the ground) is reduced due to the deposition of mud soil and the wiped-out vegetated areas. This cause decreases the depolarization phenomena over the vegetation areas, thus the surface scattering increases and volume scattering mechanism reduces. The increment in double bounce scattering mechanism can also be expected due to the exposed stems over the ground and deposited dihedral structures caused by tsunami in the vegetated/forested area. In contrast, the amount and direction of surface scattering depends on the relative permittivity, the surface roughness and the orientation of the surface [13], [29]. The deposition of urban areas debris by tsunami flow on Bragg surfaces like bare surface, agricultural fields and/or floating debris on water surface increase the surface roughness of Bragg surface for example patch B in Fig. 5. Since surface scattering provides a diversity of polarization responses, varying with an angle of incidence, dielectric constant and surface roughness/slope, the roughness leads to depolarization of the surface scattering [13], [30]. This cause reduces the surface scattering and mixes in random scattering processes in those areas, where debris was deposited by tsunami flow. The surface scattering increases over damaged areas and wiped out man-made structures (see patches C and D, Fig. 6).

Since man-made structures such as building and bridges orthogonal to radar illumination are categorized into double bounce scatterer types in the 4-CSPD scheme; the double bounce (P_d) scattering component in urban area is caused by right angle scattering between building-block-walls and road surfaces. The volume scattering (P_v) and surface scattering (P_s) components are small for orthogonally illuminated man-made structures. However, damaged or collapsed urban blocks or man-made structures resulting from the earthquake/tsunami impact that do not appear to be orthogonal to radar direction and their corresponding main scattering centre is at an oblique direction with respect to radar illumination, generate no double-bounce type effect in the 4-CSPD images after the tsunami struck. Due to multiple scattering, these red areas (pre-tsunami image) turn into green (volume scattering) in post-tsunami images. In cases, for which buildings are washed out and/or eliminated by the tsunami, those areas appear as blue surface scattering types of the 4-CSPD scheme in the post-tsunami images (see patches C and D in Fig.6). These effects in post-tsunami images as compared to pre-tsunami images provide a simple straightforward tool for interpreting collapsed buildings in tsunami affected areas. These observations are matched with ground-truth data provided by the Association of Japanese Geographers, and Geospatial Information, Authority of Japan [8], and the obtained comparisons are very convincing.

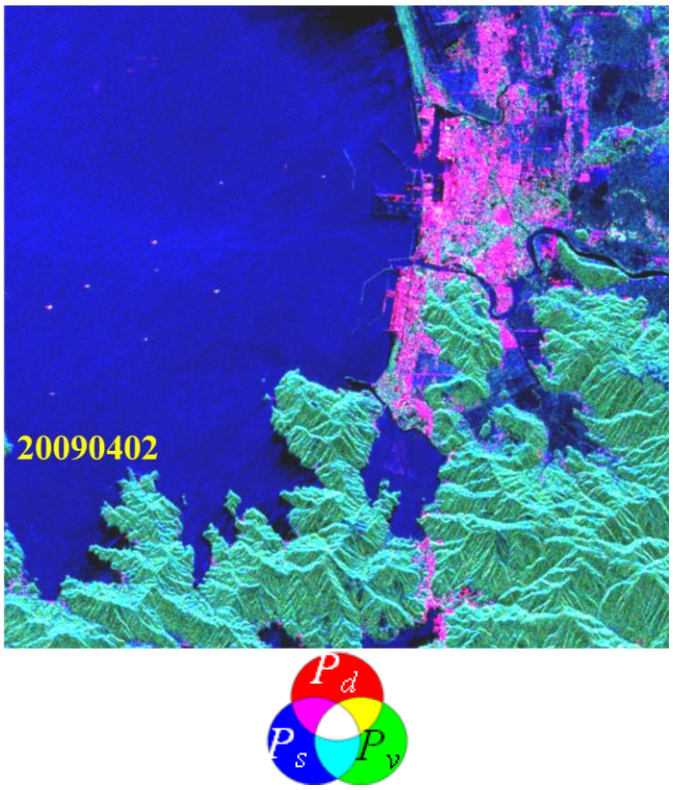

(a)

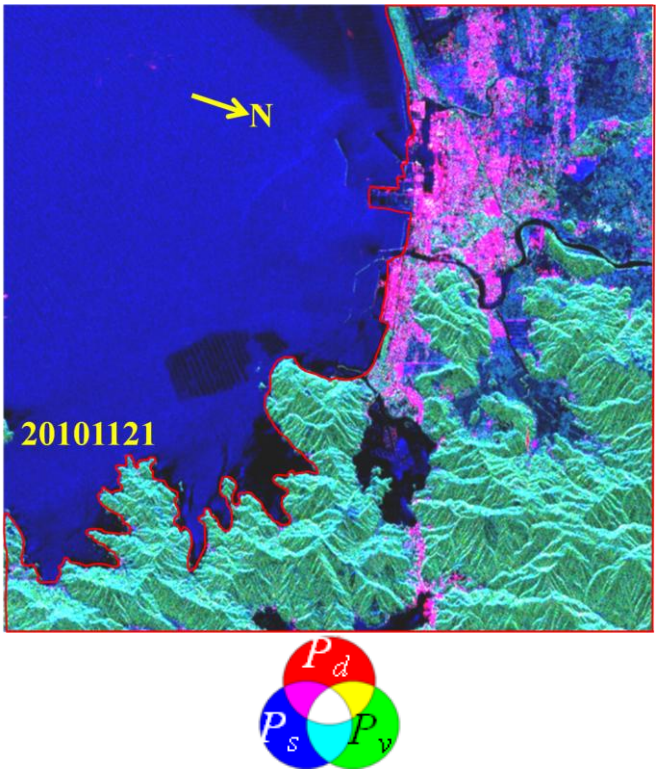

(b)

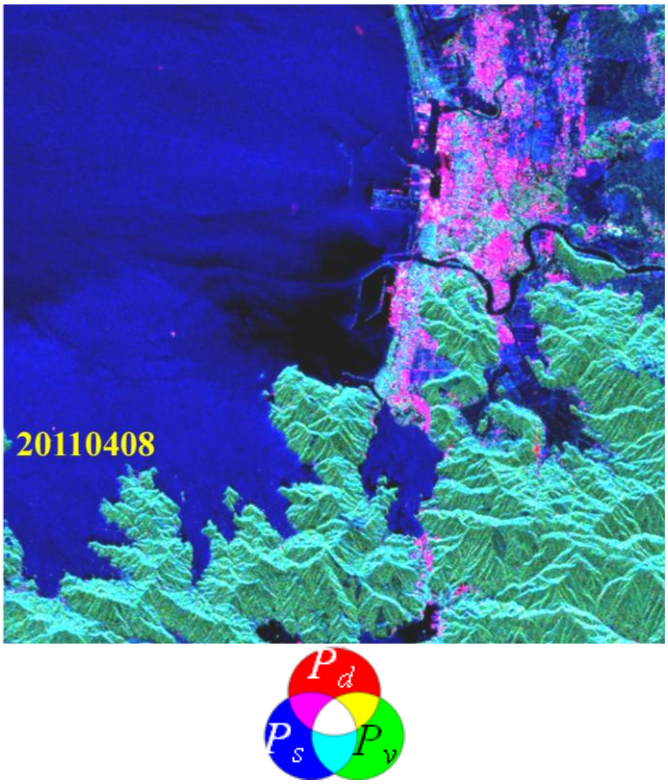

(c)

Fig. 4. Pre (a) and (b), and post (c) earthquake/tsunami 4-CSPD images for PALSAR data (In all images, the flight direction of ALSO-PALSAR is from left to right and PALSAR illumination direction is from top to bottom)

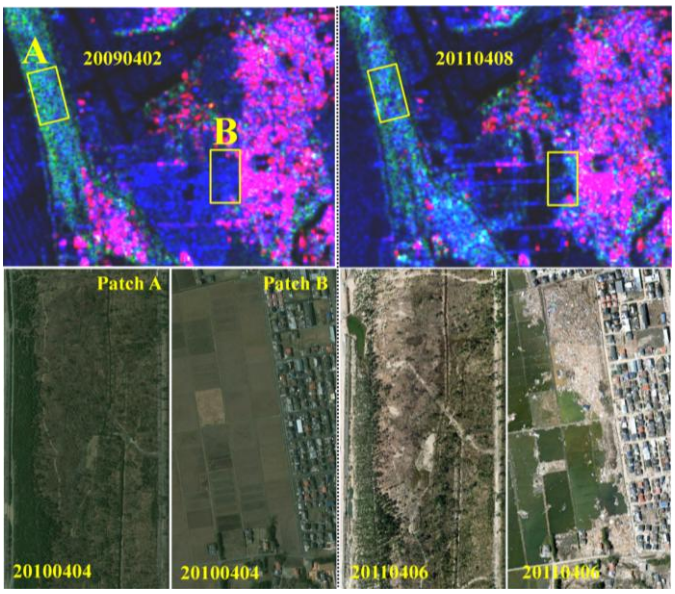

Fig. 5. Enlarged view of patch A (vegetation area) and patch B (agricultural areas) in Fig.2; **left side from black dashed line:** pre earthquake/tsunami disaster images and **right side from black dashed line:** after earthquake/tsunami images; **top row:** 4-CSPD images for the patch A and patch B and surrounding areas; and **bottom row:** Google optical images for patch A and patch B. The volume scattering (green) over the Patch A is decreased in the post disaster 4-CSPD images due to damage of forest areas as compared to pre disaster 4-CSPD images and surface scattering (blue) is increased. The surface scattering (blue) over the patch B is reduced in the post disaster 4-CSPD images due to the deposition of house debris in the agricultural areas as compared to pre disaster 4-CSPD images and the volume scattering (green) is increased.

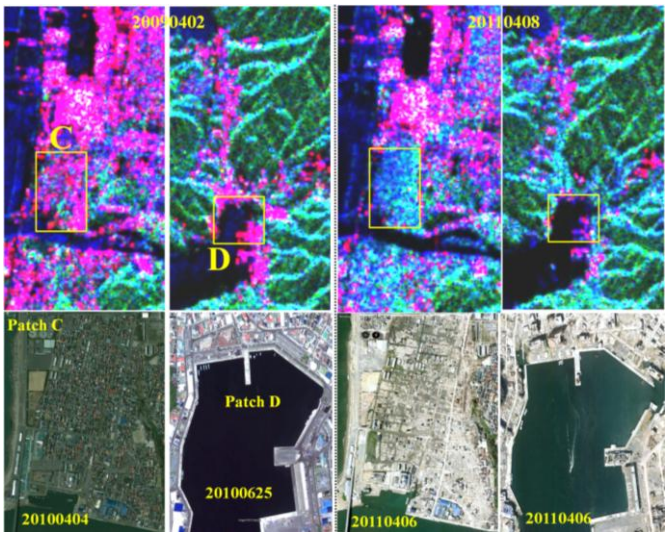

Fig. 6. Enlarged view of patch C (urban region) and patch D (urban region/ Onagawa bay) in Fig.2; **left side from black dashed line:** pre earthquake/tsunami disaster images and **right side from black dashed line:** after earthquake/tsunami images; **top row:** 4-CSPD images for the patch C and patch D and surrounding areas; and **bottom row:** Google optical images for patch C and patch D. The double bounce scattering (red) over the Patch C and the patch D is decreased in the post disaster 4-CSPD images due to the damage of buildings and houses as compared to pre disaster 4-CSPD images and surface scattering (blue) and volume scattering (green) are increased.

B. Change Analysis and Discussions

It was shown in the previous sub-section that polarimetric SAR data with 4-CSPD provided effective visual interpretation to identify the damaged areas resulting from the earthquake/tsunami disaster without difficulties from the temporal changes and seasonal changes. For the accurate and the automated change detection in urban areas to register damages caused by earthquake/tsunami disasters, it is implicit that we first need to identify the input parameters to recognize the automated changes properly. If the strategy of input parameter selection of the 4-CSPD is done properly, then this identification helps a lot to estimate the damaged areas in the urban regions. Therefore, there is need to understand and recognize the discriminating and overlapping behavior in between the temporal changes and disaster effects (pre- and post-disaster changes) on the decomposition parameters (p_s, p_v, p_d and p_c) over vegetated areas, agricultural areas, and urban areas. For example, the temporal changes [in between the 20090402 and the 20101121] and the post disaster changes [in between the pre-earthquake/tsunami (20090402) and the post-earthquake/tsunami (20110408)] in the value of the parameters p_s, p_v, p_d and p_c over the patch A (vegetated area, Fig.5), patch B (agricultural area/ wiped-out houses debris deposited area, Fig. 5), and patch C (urban region, Fig.6) are analyzed in Fig. 7, Fig. 8 and Fig. 9, respectively. Table II shows the quantitative statistics of Figs 7, 8 and 9. The temporal difference values and the difference values after the disaster in parameters p_s, p_v, p_d and p_c vary within the certain ranges as shown in Fig. 7, Fig. 8 and Fig. 9, and Table II. It is found that the mean, mode and median statistics of change are

larger in post disaster change than the temporal change and overall changes after the disaster can be separated from temporal changes based on mean, mode, and median. The mean statistics including ± standard deviation of the pixel distributions over all patches were analyzed and we observed that the parameter p_v correlated with estimated vegetation damage, the four parameters (p_s, p_v, p_d and p_c) correlated with damage and debris deposition monitoring over the agricultural areas and the parameters p_s, p_v, and p_d corresponded to the damage assessment in urban areas. But most of individual pixel difference values of temporal changes and post disaster changes are overlapping except the individual pixel difference values in p_s over patch B and p_d over patch C. Moreover, the factors for temporal and post-disaster changes are as explained in detail next.

Surface component in the vegetation area (Patch A) is particularly relevant to radar return from ground surface underneath the vegetation canopy [14]. Surface component occurs when the radar beam reaches directly to the ground through gaps in the canopy, or there is penetration of the canopy. Double bounce component in the vegetation area appears due to ground-trunk interactions. In both surface and double bounce scattering processes, the factors such as surface roughness, soil moisture, surface slope and understory vegetation layer have an important influence on radar beam interaction with ground [25],[34]. The volume scattering component is relevant to radar return from vegetation canopies due to gradual changes in dielectric constant and inhomogeneities within canopy [35] - [37]. Leaves, branches and trunks of vegetation canopy behave as attenuators [38]. The radar beam penetration depends on the density, moisture contents and structure of the vegetation canopy and presence of gaps within the canopy. If the changes are underneath the canopy, in the dielectric constant of the ground and vegetation then these changes influence the radar return. Although changes in underneath forest canopy roughness during temporal observation are not significant without natural or anthropogenic disaster activities, dielectric constant (moisture content) can vary quickly for both ground and vegetation [39]. Apart from these parameters, size, shape and orientation of the surface or canopy elements also affect the scattering components. During the maturation stage of vegetation growth, temporal variations of the parameters p_s, p_v, and p_d over the vegetation area are expected with changes either in the vegetative seasonal cycle or in the ground parameters [25],[39]. Overall, the temporal changes are somewhat barely distinguishable (see Fig.4 and Fig.7, and Table II for patch A) but after the tsunami disaster, the trends in change are understandable (see Fig.5 and Fig. 7). Since vegetation/trees were damaged by the tsunami disaster, the volume scattering decreases due to the reduction in the major sources of depolarization in scattering processes. The surface and the double bounce scattering increase over the damaged vegetated areas due to loss in stand tree density, find gaps between crowns, damage understory vegetation.

Scattering processes over a flat bare-soil surface in the agricultural field areas are affected by two attributes: (1) surface roughness, and (2) the dielectric constant of the soil medium. Due to the dynamic nature of these factors by natural or anthropogenic processes over agricultural areas, soil moisture and soil surface roughness are variables in space and time. The temporal changes in the bare agricultural field areas are anticipated due to different soil moisture and roughness conditions in the month of April, 2009 and the month of November, 2010. However the changes after the earthquake/tsunami in the agricultural field areas are envisaged due to the deposition of debris and inundation in agriculture field areas since images are used from the similar field conditions at the beginning of the month April (bare field condition). The changes after the tsunami are also confirmed due the deposition of houses debris by using high resolution Google earth images [see Fig. 5 and Fig.8, and Table II for the patch B]. The deposition of debris over the bare agricultural fields increases the roughness; this cause generates depolarization in surface scattering. As a result surface scattering is decreased and volume and double bounce scattering are greater than before the disaster condition over the debris covered areas in agricultural fields.

Temporal changes in p_s, p_v, and p_d over the urban areas are not observed to be significant because of permanent man-made structure dominance [see Fig.6 and Fig. 9, and Table II for patch C]. However, changes in p_s, p_v, and p_d, over the urban areas are noticeable after the earthquake/tsunami disaster event due to the changes in POLSAR scattering mechanism interactions with the damaged urban block and/or washed out urban block areas as compared to pre-disaster scattering behavior over the urban areas [Fig. 6 and Fig. 9 for patch C]. After the disaster, the double bounce scattering reduces due to the damage of the ground-wall and/or wall-ground interaction because radar signal is scattered in different direction as compared to before the disaster. These ground-wall and wall-ground interface over the urban areas are destroyed and/or washed out and/or reduced to debris due to the earthquake/tsunami disaster. Surface scattering becomes dominant after the disaster in those areas where the buildings are washed out by the force of the tsunami flow and leaving the ground exposed [31]. Volume scattering becomes dominant after the disaster in those areas where the buildings are oriented from the orthogonal direction with respect to the radar illumination by the force of the tsunami flow. Therefore, the value of the p_s and the p_v are increased with the earthquake and tsunami hazard compared to pre-disaster conditions over the urban areas.

When the sources of helix scattering in urban areas are damaged or changed then the scattering helicity decreases/changes in the urban areas. However, in most POLSAR measurements over vegetation areas (volume scattering dominant areas) and sea water or bare flat surfaces (Bragg surface), the reflection symmetry condition holds; but for POLSAR measurements over the double bounce scattering dominant areas (urban areas) the reflection symmetry condition does not hold [18]. So there is no remarkable advantage to use the value of the parameter p_c over the vegetation area but when the wiped-out houses and debris were deposited in the agricultural areas by the tsunami, it is found that the value of the parameter p_c increases in

agricultural area due to the loss of the reflection symmetry condition. On other hand, the value of the parameter p_c decreases in damaged urban areas.

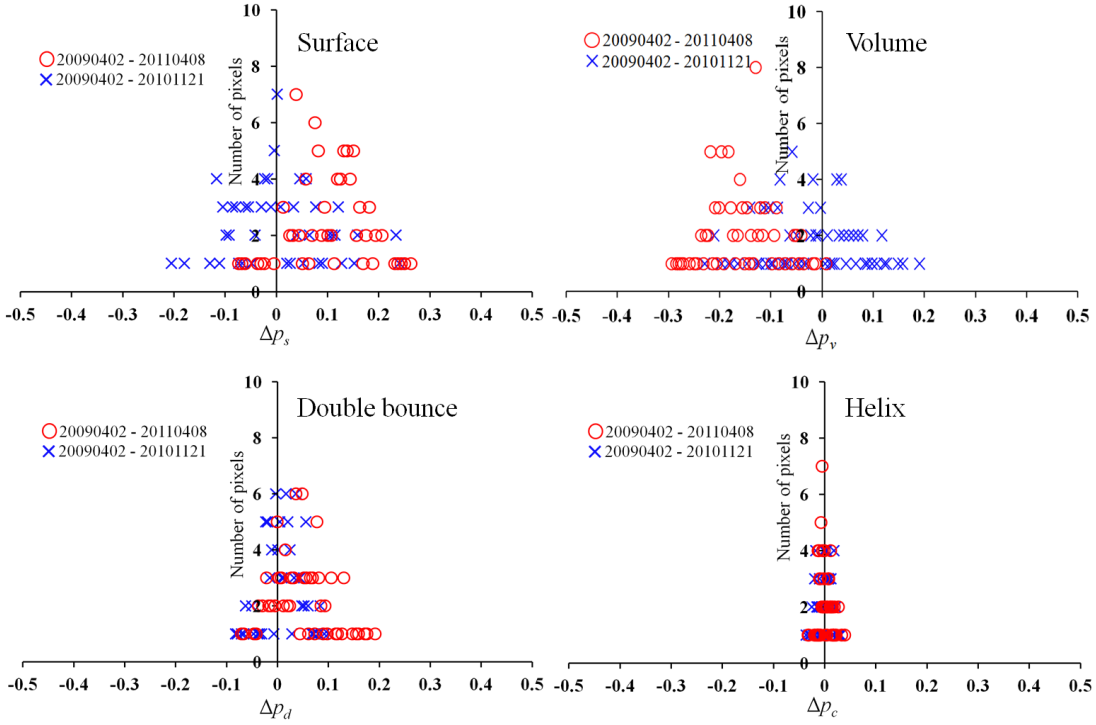

Fig. 7. Plots illustrate the differences in pixel values for the Δp_s (normalized surface scattering components difference), Δp_v (normalized volume scattering components difference), Δp_d (normalized double bounce scattering components difference), Δp_c (normalized helix scattering components difference) over vegetation, which are drawn by using a patch A (see Fig. 5) [○ denotes the difference in between pre- earthquake/tsunami (20090402) and post-earthquake/tsunami (20110408) decomposition parameters; and × denotes temporal difference [before (20090402) –after (20101121)] of the decomposition parameters]

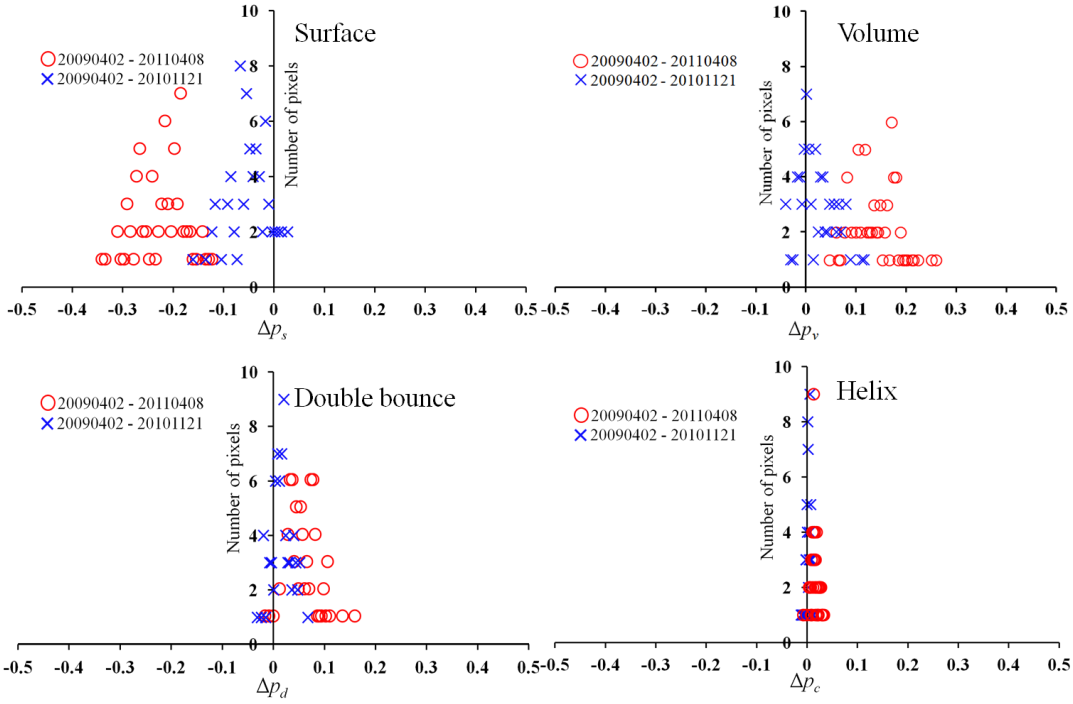

Fig. 8. Plots illustrate the differences in pixel values for the Δp_s , Δp_v , Δp_d , Δp_c over agricultural area/ debris on agricultural area, these plots are plotted by using a patch B (see Fig. 5) [○ denotes the difference in between pre- earthquake/tsunami (20090402) and post-earthquake/tsunami (20110408) decomposition parameters; and × denotes temporal difference [before (20090402) –after (20101121)] of the decomposition parameters]

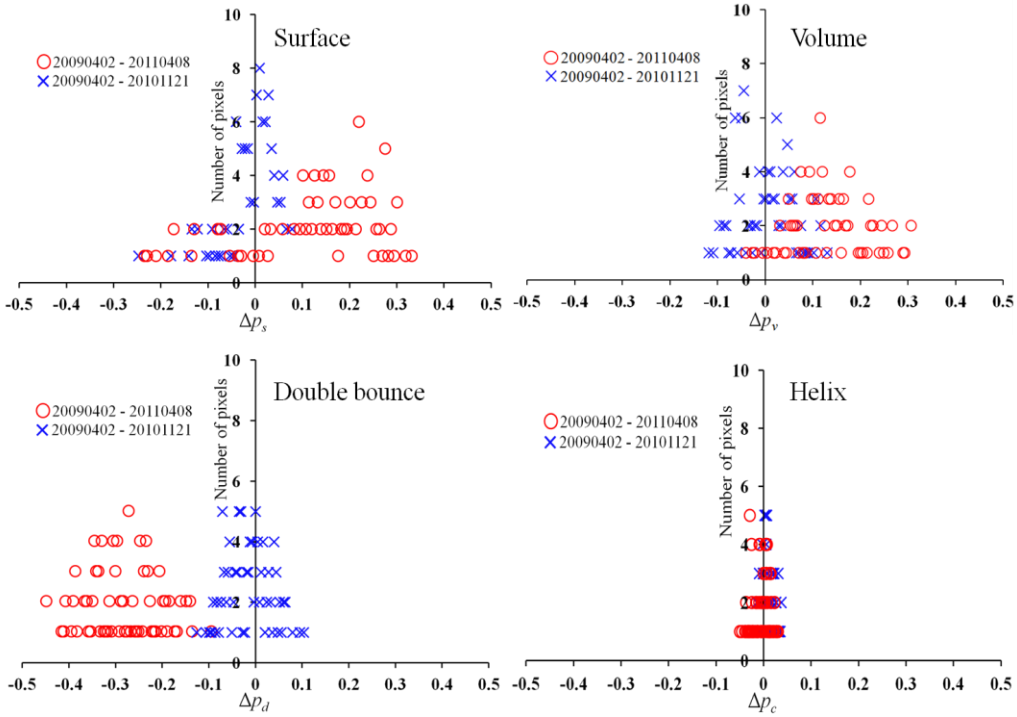

Fig. 9. Plots illustrate the differences in pixel values for the Δp_s , Δp_v , Δp_d , Δp_c over urban area, these plots are drawn by using a patch C (Fig. 6) [○ denotes the difference in between pre- earthquake/tsunami (20090402) and post-earthquake/tsunami (20110408) decomposition parameters, and also × denotes temporal difference [before (20090402) –after (20101121)] of the decomposition parameters]

Table II. Statistics of the difference values of pixels for patches A, B and C [○ denotes the difference in between pre- earthquake/tsunami (20090402) and post-earthquake/tsunami (20110408) decomposition parameters, and also × denotes temporal difference [before (20090402) –after (20101121)] of the decomposition parameters]

	Scattering component		Min.	Max.	Mean	Median	Mode	Std. Dev.	Number of pixels
	Δp_s	○	-0.073	0.263	0.107	0.107	0.038	0.070	
Patch A		×	-0.204	0.240	0.007	-0.004	0.002	0.087	
	Δp_v	○	-0.299	0.008	-0.154	-0.160	-0.129	0.066	
		×	-0.229	0.189	-0.022	-0.022	-0.058	0.088	
	Δp_d	○	-0.067	0.192	0.047	0.036	0.036	0.054	
		×	-0.083	0.099	0.013	0.012	0.012	0.038	100
	Δp_c	○	-0.032	0.038	-0.000	0.000	-0.018	0.015	
		×	-0.036	0.030	0.001	-0.001	-0.005	0.013	
Patch B	Δp_s	○	-0.341	-0.123	-0.222	-0.216	-0.185	0.050	
		×	-0.160	0.027	-0.046	-0.048	-0.066	0.039	
	Δp_v	○	0.048	0.262	0.145	0.142	0.173	0.046	
		×	-0.040	0.116	0.024	0.019	0.001	0.035	75
	Δp_d	○	-0.017	0.158	0.061	0.056	0.032	0.031	
		×	-0.031	0.068	0.019	0.016	0.020	0.020	
	Δp_c	○	-0.008	0.033	0.016	0.014	0.012	0.008	
		×	-0.012	0.020	0.004	0.003	0.005	0.005	
Patch C	Δp_s	○	-0.235	0.331	0.136	0.157	0.219	0.132	
		×	-0.248	0.140	-0.001	0.008	0.062	0.002	
	Δp_v	○	-0.040	0.355	0.150	0.128	0.115	0.093	
		×	-0.118	0.130	0.005	0.005	-0.045	0.056	
	Δp_d	○	-0.445	-0.095	-0.280	-0.288	-0.272	0.075	112
		×	-0.126	0.175	-0.012	-0.015	-0.070	0.050	
	Δp_c	○	-0.050	0.030	-0.006	-0.003	-0.028	0.018	
		×	-0.270	0.036	0.007	0.005	0.001	0.014	

Furthermore, the changes for the red line boundary areas in Fig. 4(b) in the value the parameters p_s, p_v and p_d [in between the pre- earthquake/tsunami (20090402) and post-earthquake/tsunami (20110408)] are categorized in Figs. 10(a), 10(b) and 10(c), respectively. The value of the p_s increases 0.1 to 0.3 in distorted ocean-shore vegetation areas and agricultural areas while the value of p_v of those areas decreases. A decrement of more than 0.1 in the value of the p_s is also noticed in those areas containing wiped-out houses and debris deposited by tsunami flow (e.g., patch B) and the washed-out houses debris floating in bay areas, e.g., in the water areas of patch D. Moreover, it was observed that the value of the parameter p_v decreases by more than 0.1 in the damaged vegetated area by the tsunami impact, nevertheless

temporal/seasonal changes in land cover (which is not affected by the tsunami) overlap with tsunami affected areas. The value of the p_d over the collapsed or wiped-out buildings is decreased while that of distorted vegetation areas along the ocean-shore is increased upto 0.1 as compared to pre-disaster conditions. The value of p_d over the vegetation and the agricultural areas is found to be ±0.1 and also mixed with the non-tsunami-covered areas. The value of the parameter p_d increase from 0.1 to 0.3 for locations where the wiped-out houses were deposited in the agricultural areas and/or floated in bay areas.

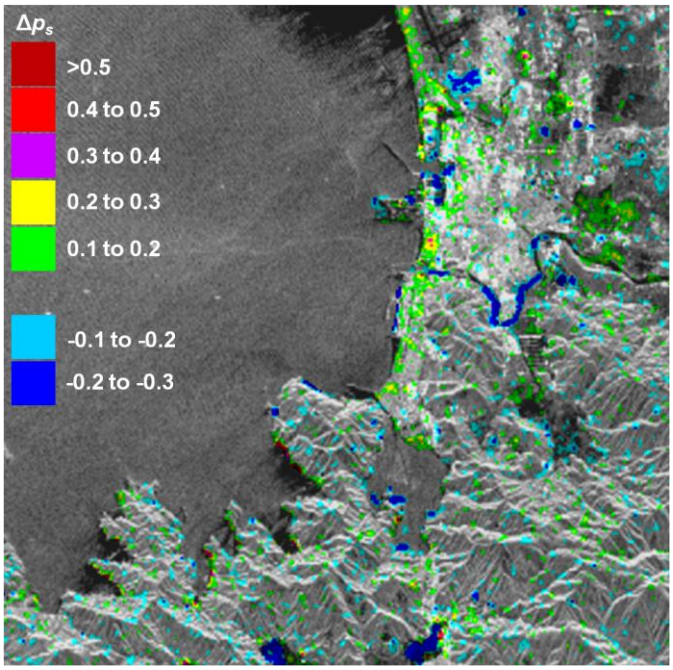

(a)

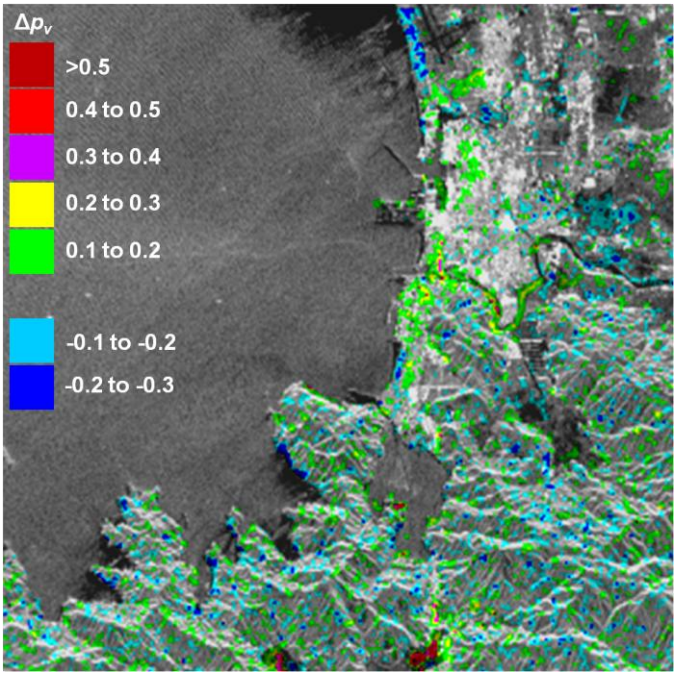

(b)

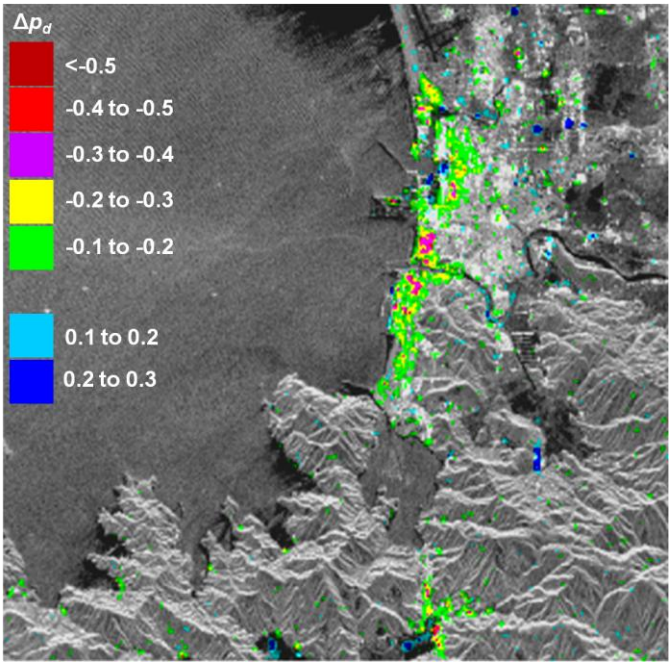

(c)

Fig. 10. The difference images in between pre-earthquake/tsunami (20090402) and post-earthquake/tsunami (20110408) behavior of decomposition parameters (a) Δp_s , (b) Δp_v and (c) Δp_d are superimposed on *TP* image of 20090402.

As the comparisons of the 4-CSPD RGB in Fig.4 and the pixel distribution plots in Fig.9 show that the dominate double bounce scattering contribution (red color in Fig. 4) in between 20090402 and 20101121 is not significantly changed and the difference value only slightly changes within the range ±0.1. This slight temporal change ±0.1 in the p_d is because of that the seasonal change could be sustained in minor natural scatterers e.g. tree or vegetation [39], which are mixed with urban blocks in resolution cells. The change of season affects the moisture content of vegetation and soil, which in turn influences the intensity of radar backscatter and settlement detectability. This cause fluctuates the difference value of p_d but this change in p_d is small as compared to change after the earthquake/tsunami. Moreover, a few spots show temporal changes of more than 0.1 in p_d over the car parking areas, small agricultural land in urban area and those building close to agricultural areas, the effect of agricultural land on settlement detectability implies variability with climatic season. Otherwise changes of more than 0.1 in p_d over urban blocks and other areas containing man-made structures are less sensitive to temporal changes (Fig.11). However, the same season's images are utilized to minimize effect of the seasonal cycle changes in the urban area.

Furthermore, it is well illustrated in the pertinent literatures [9] – [20] that the double bounce scattering over the urban area becomes dominant because of the ground-building wall interface or the building wall–ground interface and other-man-made structures. Building blocks in the urban areas can be treated as relatively coherent scatterers [9], which do not change with time unless natural and/or anthropogenic disaster occurrence. When these wall-ground and ground-wall

interfaces are damaged by the earthquake/tsunami disaster, the reduction in the amount of the double bounce scattering power will be noticed. Since a difference of the p_d value in between pre- and post-disaster is very sensitive for man-made structures, the parameter p_d is useful to analyze the influence of earthquake and tsunami before and after the natural hazard event. Further these changes in the parameter p_d are related to the urban areas affected by the earthquake and tsunami. For example, the difference of the p_d value in between pre and post-disaster is categorized over the Ishinomaki city and surrounding areas and it is observed that green color (-0.1 to -0.2) coded areas in Fig. 12 appears in urban areas for partly damaged buildings and/or made-structures; whereas yellow (-0.2 to -0.3), magenta (-0.3 to -0.4), red (-0.4 to -0.5) and brown (< -0.5) colors in Fig. 12 represent the severely damaged urban areas and/or areas with completely wiped-out houses by earthquake/tsunami impacts.

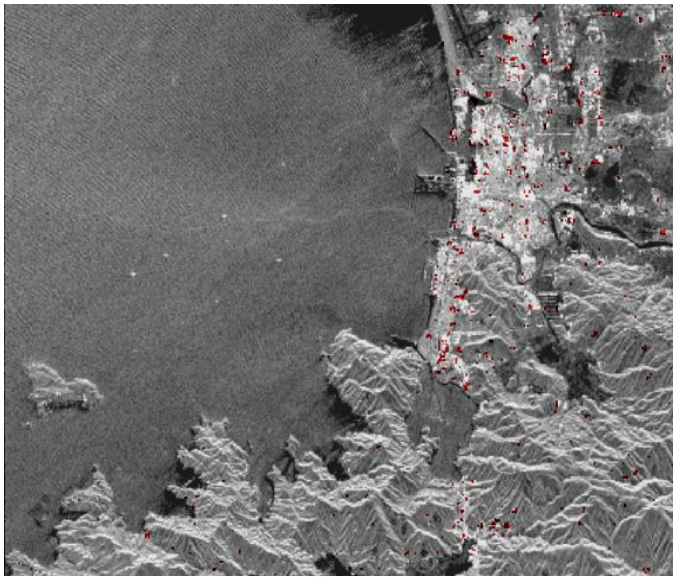

Fig. 11. The masked temporal difference (in between the 20090402 and 20101121) of the decomposition parameter Δp_d image is superimposed on the *TP* image of 20090402 [brown color denotes the difference < -0.1].

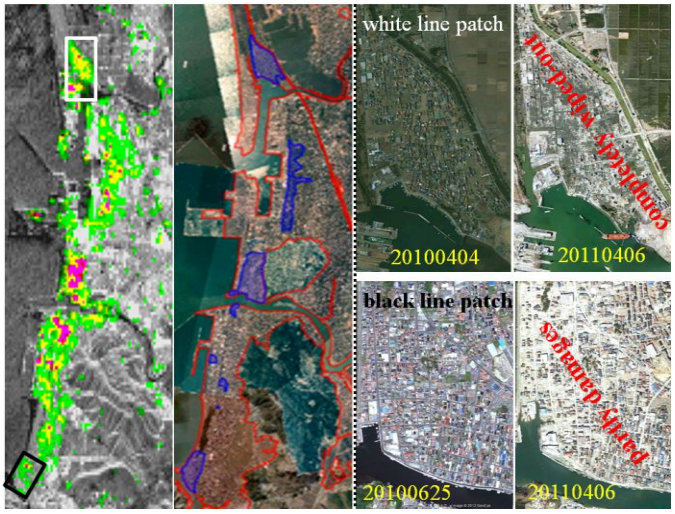

Fig. 12. **Left:** the masked temporal difference (in between the 20090402 and 20101121) of decomposition parameter Δp_d image is superimposed on *TP* image of 20090402 [green color represents partly damages in urban areas, and yellow, magenta, red and brown color denote the completely wiped out urban areas]; **second image from left:** ground truth information [blue color areas show damages in urban areas and red color represents tsunami covered areas]; and **right side from the black dashed line:** Google optical pre- and post-earthquake/tsunami the upper optical images for white line patch on left-side image and the lower optical images for black line patch on left-side image, respectively.

C. VHR SAR Color-Coded Images

The high resolution quad polarization PALSAR images showed their capability in the detection and analysis of urban areas. In addition, VHR quad polarization synthetic aperture radar (SAR) sensors permit to extract information from VHR SAR images about the man-made and natural features individually. Unfortunately, we do not have polarimetric VHR image data sets over the Off-Tohoku Tsunami/earthquake coastal areas; but we have VHR fully polarimetric POLSAR image data access over the other parts of the globe. These data sets cover various features such as urban areas, vegetation, water areas, etc. This section shows that VHR SAR images (TerraSAR-X images) provide better decomposition images over highly oriented man-made features and urban areas as compared to standard resolution images (e.g. PALSAR images). Therefore, polarimetric VHR imagery should provide more accurate damage assessments of natural occurring and anthropogenic hazards in dense urban areas. For example, the high resolution ALOS-PALSAR and VHR TerraSAR-X quad-polarization data sets were used over Niigata, Japan for comparing the effect of resolution with the 4-CSPD scheme [21]. High resolution ALOS-PALSAR quad polarization data were acquired on March 04, 2010 with 21.5^0 off-nadir angle and VHR TerraSAR-X quad polarization data were acquired on April 22, 2010 with 36.7^0 off nadir angle. For TerraSAR-X data sets, the window size for the ensemble average in image processing was chosen as 12 in the range direction and 10 in the azimuth direction. The 4-CSPD color-coded images of ALOS-PALSAR and TerraSAR-X over the Niigata are displayed in Fig. 13 and Fig 14. The VHR (2 meter ground range resolution) quad polarization TerraSAR-X data with the 4-CSPD method clearly envisages urban areas compared to high resolution (30 meter ground range resolution) ALOS-PALSAR data. Additionally, a representative VHR F-SAR S-band image of June 08, 2010 over the Kaufbeuren, Germany is shown in Fig. 15 with the 4-CSPD method, the VHR resolution (0.5 meter) provides the information on individual buildings and single trees. The F-SAR images were averaged by factor 10 in the both range direction and the azimuth direction before generating the 4-CSPD color-coded image. The comparison of the Pauli and 4-CSPD RGB in Fig. 16 showed that objects discriminations are visible in the 4-CSPD RGB much clearer. Moreover, it becomes apparent that using VHR quad polarization SAR images and implementing the 4-CSPD method improves rather considerably the discrimination of the land-use/land-cover objects from one another.

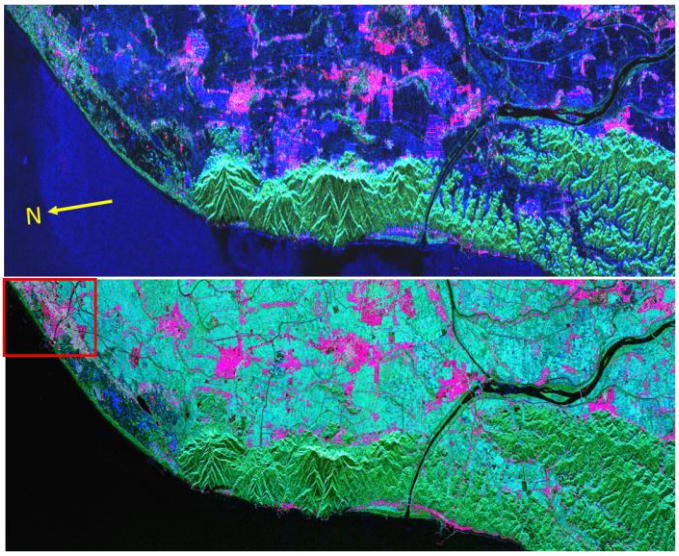

Fig.13. The 4-CSPD color-coded images with surface scattering (blue), volume scattering (green) and double bounce scattering (red) over the Niigata, Japan (top) ALOS-PALSAR data of March 03, 2010 (bottom) TerraSAR-X data of April 22, 2010.

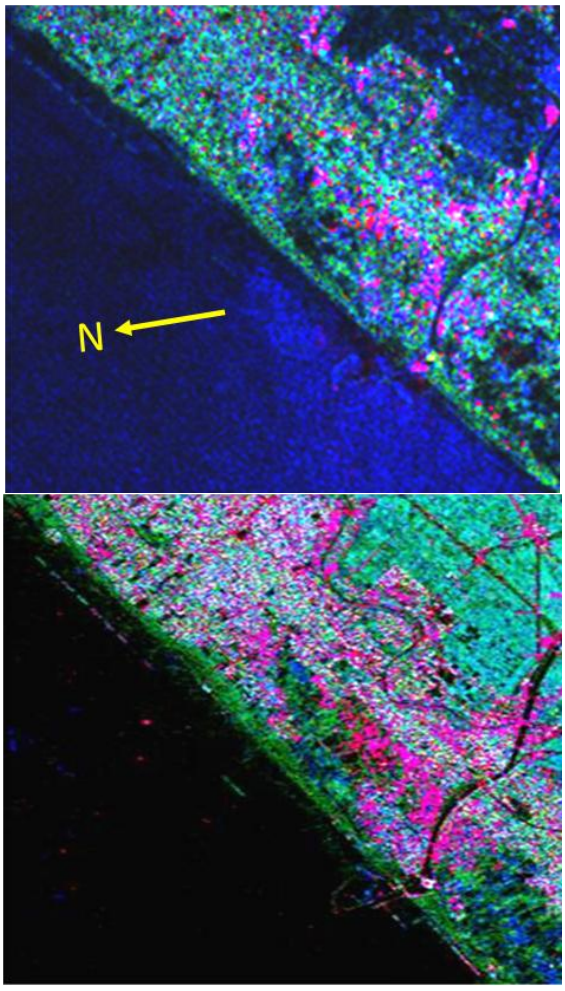

Fig.14. Close-up of the 4-CSPD color-coded images with surface scattering (blue), volume scattering (green) and double bounce scattering (red) over the Niigata, Japan for red rectangular areas in Fig. 13 (top) ALOS-PALSAR (bottom) TerraSAR-X.

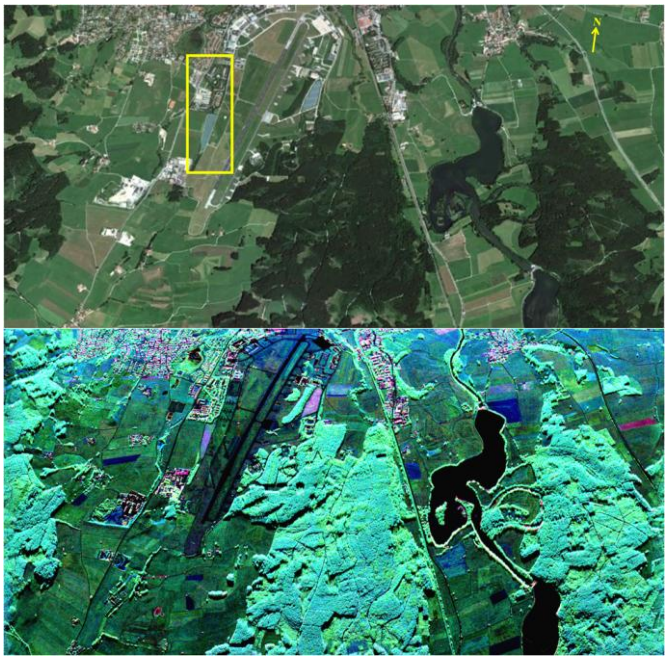

Fig.15. (top) Google optical image of July 16, 2010 and (bottom) The 4-CSPD color-coded image for DLR F-SAR S-band data of the June 08, 2010 with surface scattering (blue), volume scattering (green) and double bounce scattering (red) over the Kaufbeuren, Germany

Fig.16. Close-up area of yellow line box in Fig.15 (left) Google optical image of July 16, 2010; (center) Pauli RGB HH-VV (red), 2HV (green), HH+VV (blue) image and (right) the 4-CSPD color-coded image for DLR F-SAR S-band data of the June 08, 2010 with surface scattering (blue), volume scattering (green) and double bounce scattering (red) over the Kaufbeuren, Germany

IV. CONCLUSIONS

Fully polarimetric high resolution L-Band image data sets with the implementation of the 4-CSPD scheme provide a straight forward simple tool for interpreting as well as identifying collapsed buildings caused by earthquake/ tsunami disasters. This result holds equally well for typhoon or tornado and other manmade disaster assessments. Furthermore, the basic behaviors of scattering parameters p_s , p_v and p_d are

observed as follows: (1) generally, the surface scattering is increased in tsunami affected areas (vegetation damaged area and wiped-out/collapsed urban block area) but it can be decreased in the areas of the deposition of wiped-out houses by the retreating tsunami and for the floating houses on bay areas. (2)The volume scattering is decreased in tsunami affected or damaged vegetation areas and increased in damaged or collapsed, deposited and/or floating (on bays water surface) urban blocks or man-made structures by the earthquake/tsunami. (3) The double bounce scattering is decreased in earthquake/tsunami collapsed or damaged urban areas and increased in areas with deposited (in agricultural field or other type scattering dominate areas) or floating (on bays water surface) wiped-out urban blocks or man-made structures, mainly caused by the retreating tsunami.

Here, we need to emphasize that based on reproducible multi-band FSAR experiments carried out at DLR [40], the S-Band fully polarimetric POLSAR image data sets will be superior to L-band because at S-Band higher resolution and still high polarimetric sensitivity can be achieved which for L-Band does not yield such high resolution although polarimetric sensitivity is high. The C-Band polarimetric sensitivity is inferior to S-Band and the resolution is not remarkably increased. Furthermore, currently the S-Band operational bandwidth is still relatively larger for satellite implementation of fully polarimetric VHR POLSAR sensors. Therefore, we are looking forward to the addition of a high resolution fully polarimetric S-Band POLSAR satellite sensors for improved VHR POLSAR natural and also anthropogenic in situ disaster damage assessment.

ACKNOLEDGEMENTS

The authors are grateful to JAXA-EORC for providing ALOS-PALSAR data sets under RA No 599 and also to Association of Japanese Geographers, and Geospatial Information, Authority of Japan for providing ground truth data. In addition, we express our sincere gratitude for being provided the excellent VHR X-Band TerraSAR-X and S-Band F-SAR fully polarimetric POLSAR image data sets by DLR Oberpfaffenhofen, Germany.

REFERENCES

[1] F. Yamazaki, and M. Matsuoka, “Remote sensing technologies in post-disaster Damage assessment,” *Journal of Earthquake and Tsunami*, vol. 01, no. 03, pp. 1-17, 2007.

[2] D. Brunner, G. Lemoine, and L. Bruzzone, “Earthquake damage assessment of buildings using VHR optical and SAR imagery,” *IEEE Trans. Geosci. Remote Sens.*, vol. 48, no. 5, pp. 2403-2420, May 2010.

[3] M. Matsuoka, and S. Koshimura, “Tsunami damaged area estimation for the 2010 Maule, Chile earthquake using ASTER DEM and PALSAR images on the geo grid,” *8th Int. Workshop on Remote Sens. and Disaster Response* on Sept. 30- Oct. 1, 2010, Tokyo, Japan, 2010.

[4] M. Chini, N. Pierdicca, W. J. Emery, “ exploiting SAR and VHR optical images to quantify damages caused by the 2003 Bam earthquake,” *IEEE Trans. Geosci. Remote Sens.*, vol. 47, no. 1, pp. 145-152, Jan. 2009.

[5] C. Yonezawa, and S. Takeuchi, “ Decorelation of SAR data by urban damage caused by the 1995 Hoyogoken-Nanbu earthquek”, *Int. J. Remote Sens.*, vol. 22, no. 8, pp. 1585-1600, 2001.

[6] M. Matsuoka, and F. Yamazaki, “ Use of satellite SAR intensity imagery for detecting building areas damaged due to earthquakes, *Earthquake Spectra*, vol. 20, no. 3, pp. 975-994, 2004.

[7] Damage Situation and Police Countermeasures associated with 2011Tohoku district - off the Pacific Ocean Earthquake on September 10, 2012, National Police Agency of Japan. (Accessed 2012-09-11).

[8] Geospatial Information Authority of Japan (accessed 2011-06-17). [Online]. Available: http://www.gsi.go.jp

[9] H. Mott, *Remote sensing with polarimetric radar*, John wiley and sons, Inc., Hoboken, New Jersey, USA, 2007.

[10] J. S. Lee and E. Pottier, Polarimetric radar imaging from basics to applications, CRC Press, 2009.

[11] W. M. Boerner , H. Mott , E. Luneburg , C. Livingstone , B. Brisco , R.J. Brown, J.S. Paterson, S.R. Cloude, E. Krogager, J.S. Lee, D.L. Shuler, J.J. Van zyl , D. Randall , P. Budkewitsch and E. Pottier, “Polarimetry in radar remote sensing: basic and applied concepts,” In *Manual of remote sensing: principles and applications of Imaging Radar*. Edited by F. M. Henderson and A. J. Lewis. John Wiley & Sons, Inc. *New York*. vol. 2, ch.5, pp. 271-356, 1998.

[12] R. Touzi, W M Boerner, J S Lee, E. Lueneburg, “A review of polarimetry in the context of synthetic aperture radar: concepts and information extraction”, *Can. J. Remote Sens.*, vol. 30, no. 3, pp. 380-407, 2004.

[13] S. R. Cloude, *Polarisation: Applications in Remote Sensing*. London, U.K.: Oxford Univ. Press, 2009.

[14] A. Freeman and S. Durden, "A three-component scattering model for polarimetric SAR data," IEEE Trans. Geosci. Remote Sens., vol. 36, no. 3, pp. 963-973, May 1998.

[15] Y. Yamaguchi, T. Moriyama, M. Ishido, and H. Yamada, "Four-component scattering model for polarimetric SAR image decomposition," IEEE Trans. Geosci. Remote Sens., vol. 43, no. 8, pp. 1699-1706, Aug. 2005.

[16] Yajima, Y. Yamaguchi, R. Sato, H. Yamada, and W. -M. Boerner, “POLSAR image analysis of wetlands using a modified four-component scattering power decomposition,” IEEE Trans. Geosci. Remote Sens., vol. 46, no. 6, pp. 1667-1773, June 2008.

[17] J. S. Lee and T. Ainsworth, “The effect of orientation angle compensation on coherency matrix and polarimetric target decompositions,” *IEEE Trans. Geosci. Remote Sens.*, vol. 49, no. 1, pp. 53-64, Jan. 2011.

[18] Y. Yamaguchi, A. Sato, W.-M. Boerner, R. Sato, and H. Yamada, “Four-component scattering power decomposition with rotation of coherency matrix,” *IEEE Trans. Geosci. Remote Sens.*, vol. 49, no. 6, pp. 2251-2258, Jun. 2011.

[19] A. Sato, Y. Yamaguchi, G. Singh, S.-E. Park, “Four-component scattering power decomposition with extended volume scattering model,” *IEEE Geosci. Remote Sens. Lett.*, vol. 9, no. 2, pp. 166 – 170, Mar. 2012.

[20] G. Singh, Yoshio Yamaguchi, S.-E. Park, Yi Cui and H. Kobayashi “Hybrid Freeman/eigenvalue model with extended volume scattering model”, *IEEE Geosci. Remote Sens. Lett*, vol. 10, no. 1, pp. 81-85, 2013.

[21] G. Singh, Y. Yamaguchi, Yi Cui, S.-E. Park, R. Sato, “New four component scattering power decomposition method,” in *Proc. EUSAR 2012 - 9th European Conference on Synthetic Aperture Radar*, April 23-26, 2012, Nuremberg, Germany.

[22] Y. Yamaguchi, G. Singh, S.-E. Park and H. Yamada, “Scattering power decomposition using fully polarimetric information,” in *Proc. IEEE IGRASS*, Munich, Germany, July 22-27, 2012, pp.91-94.

[23] S. O. Rice, ‘‘Reflection of Electromagnetic Waves from Slightly Rough Surfaces,’’ *Communications on Pure and Applied Mathematics*, vol. 4, pp. 361–378, 1951.

[24] J. J. van Zyl, “Unsupervised classification of scattering behavior using radar polarimetry data,” *IEEE Trans. Geosci. Remote Sens.*, vol. 27, no. 1, pp. 36-45, Jan.1989.

[25] F.T. Ulaby, R. K. Moore and A.K. Fung, *Microwave remote sensing, active and passive, from theory to applications.* Vol. III, Addison-Wesley Publishing Company: Reading, 1986.

[26] P. Beckmann and A. Spizzichino, *The Scattering of Electromagnetic Waves from Rough Surfaces*, Artech House, Norwood, Massachusetts, 1987.

[27] A. K. Fung, Z. Li, and K. S. Chen, “Backscattering from a Randomly Rough Dielectric Surface,” *IEEE Transactions on Geoscience and Remote Sensing*, vol. 30, pp. 356–369, 1992.

[28] J. van Zyl , and Y. Kim, *Synthetic Aperture Radar Polarimetric*, Wiley, USA, 2011.
[29] W. H. Peake and T. L. Oliver, *The Response of Terrestrial Surfaces at Microwave Frequencies*, Technical Report AFAL-TR-70301, Electroscience Laboratory, Ohio State University, Columbus, Ohio, 1971.
[30] I. Hajnsek, E. Pottier, and S. R. Cloude, "Inversion of surface parameters from polarimetric SAR," *IEEE Trans. Geosci. Remote Sens.*, vol. 41, no. 4, pp. 727-744, Apr. 2003.
[31] Gulab Singh, Osamu Simotoso, Sang-Eun Park, Yoshio Yamaguchi Monitoring of the 2011 Tohoku Earthquake and Tsunami Disaster using SAR Polarimetry Techniques, *IEICE Tech. Rep.*, vol. 111, no. 177, SANE2011-59, pp. 21-24, Aug. 2011.
[32] S.V. Nghiem, S.H. Yueh, R. Kwok and F.K. Li, "Symmetry properties in polarimetric remote sensing," *Radio Science*, vol. 27, no. 5, pp. 693 711, Oct. 1992.
[33] K. Kitayama, Y. Yamaguchi, J. Yang and H. Yamada, "Compound scattering matrix of targets aligned in the range direction," *IEICE Trans. Commun.*, vol. E84-B, no.1, Jan. 2001.
[34] D.G. Leckie and K. J. Ranson, "Forestry applications using imaging radar," In *Manual of remote sensing: principles and applications of Imaging Radar*. Edited by F. M. Henderson and A. J. Lewis. John Wiley & Sons, Inc. *New York*. vol. 2, ch.9, pp. 435-509, 1998.
[35] R. Zoughi, L.K. Wu and R.K. Moore, "Identification of major backscattering sources in trees and shrubs at 10GHz," *Remote Sens. Environ.*, vol. 19, no. 3, pp. 269-290, 1986.
[36] S. L. Durden, J. J. van Zyl, and H. A. Zebker, "Modeling and observation of the radar polarization signature of forested areas," *IEEE Tans. Geosci. Remote Sens.*, vol. 27, no. 3, pp. 290-301, Mar. 1989.
[37] S. L. Durden, J. J. van Zyl, and H. A. Zebker, "The unpolarized component in polarimetric radar observations of forested areas," *IEEE Tans. Geosci. Remote Sens.*, vol. 28, no. *2*, pp. 268-271, Feb. 1990.
[38] N.S. Chauhan and R.H. Lang, "Polarization utilization in the microwave inversion of leaf angle distributions", *IEEE Trans. Geosci. Remote Sens.*, vol. 27, no. 4, pp. 395-402, Apr. 1989.
[39] M.C. Dobson, L. Pierce, K.C. Mc. Donald and T. Sharik, "Seasonal change in radar backscatter from mixed conifer and hardwood forests in northern Michigan", *Proc. Int. Geosci. Remote Sens. Symp.'91*, pp. 1121-1124, 1991.
[40] A. Reigber, M. Jäger, J. Fischer, R. Horn, R. Scheiber, P. Prats, and A. Nottensteiner, "System status and calibration of the F-SAR air-borne SAR instrument," *Proc. IGARSS 2011*, Vancouver, BC, 2011 August, pp.1520 - 1523.

Gulab Singh (S'09-M'10) was born in Salooni-Sarsawa-Saharanpur, Uttar Pradesh, India in 1976, received his B.Sc. and M.Sc. degrees in physics from the Choudhary Charan Singh University (formerly Meerut University), Meerut, India in 1998 and 2000, respectively, and his M. Tech. degree in remote sensing from the Birla Institute of Technology, Ranchi, India in 2005 and his Ph.D. from Indian Institute of Technology Bombay, Mumbai, India in 2011. He has honoured with the "*Award for Excellence in Thesis Work*" for his outstanding research contributions from Indian Institute of Technology Bombay, Mumbai, India on 5th August, 2011. From 2002 to 2030, he was a Physics lecturer at Janta Inter College Jhabiran, Saharanpur, Uttar Pradesh, India. From 2005 to 2007, he was Senior Research Fellow at Centre of Studies in Resources Engineering, Indian Institute of Technology Bombay, Mumbai, India, where he was involved in several research projects related to POL-SAR and In-SAR data analysis for snow and ice parameters retrieval. From April 2010, he is Post Doctoral Fellow at Graduate School of Science and Technology, Niigata University, Niigata, Japan. His current research interests include SAR data analysis, SAR polarimetry and SAR interferometry techniques development for earth and lunar surface parameters estimation.

Yoshio Yamaguchi (M'83-SM'94-F'02) received the B.E. degree in electronics engineering from Niigata University, Niigata, Japan, in 1976, and the M.E. and Dr. Eng. degrees from the Tokyo Institute of Technology, Tokyo, Japan, in 1978 and 1983, respectively. In 1978, he joined the Faculty of Engineering, Niigata University. From 1988 to 1989, he was a Research Associate at the University of Illinois at Chicago, Chicago. He is currently with the Graduate School of Science and Technology, Niigata University. His interests are in the field of radar polarimetry, microwave sensing, and imaging.
Dr. Yamaguchi has served as Chair of IEEE Geoscience & Remote Sensing Society (GRSS) Japan Chapter (2002–2003), Chair of International Union of Radio Science Commision F Japanese Committee (URSI-F) Japan (2006–2011), Associate Editor for Asian affairs of GRSS Newsletter (2003–2007), and Technical Program Committee (TPC) Co-Chair of the 2011 IEEE International Geoscience and Remote Sensing Symposium (IGARSS). He is a Fellow of the Institute of Electronics, Information and Communication Engineers (IEICE), Japan, and a recipient of the 2008 IEEE GRSS Education Award.

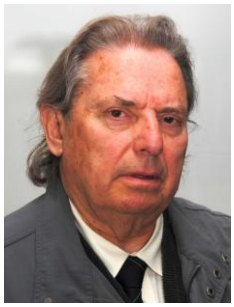

Wolfgang-Martin Boerner (SM'75-F'84, LF'92) was born in Finschhafen, Papua New Guinea in 1937, received the B.S. (Abitur) degree from the August von Platen Gymnasium, Ansbach, Germany, the M.S. (Dipl.-Ing.) degree from the Technical University of Munich, Bavaria, Germany, and the Ph.D. degree in Electromagnetic Engineering Sciences from the Moore School of Electrical Engineering at the University of Pennsylvania, Philadelphia, in 1958, 1963, and 1967, respectively.
From 1967 to 1968 he was a Research Assistant Engineer with the EECS Radiation Laboratory of the University of Michigan, Ann Arbor, MI. In 1968 he joined the University of Manitoba at Winnipeg, Canada where he was strongly active in across-Canada research activities on the advancement of inverse problems in aeronomy and radar remote sensing and surveillance. Since 1978, he has been a Professor at the Department of Electrical & Computer Engineering (formerly EECS), the University of Illinois at Chicago, and Director of its Communications, Sensing and Navigation Laboratory. While at UIC Professor Boerner was awarded the Alexander von Humboldt Senior US Scientist, the Japan Society for the Promotion of Science Senior US Scientist, and the US Navy Distinguished Senior Professor awards; he is now a University of Illinois Distinguished Senior Professor Emeritus, and he was awarded the *Doctor Honoris Causa* (Dr. H. C.) of the Tomsk State University Cluster in Tomsk, West Siberia on 2000 October 12, of the University of Rennes 1, Bretagne, France on 2003 April 04, and of the Friedrich-Alexander-University of Erlangen-Nuremberg, Germany on 2003 April 11 - all in recognition for his profound contributions to the advancements of Electromagnetic Vector Inverse Scattering, Radar Polarimetry, Interferometry and Tomography. He is a Corresponding Member of the Saxonian Academy of Science at Leipzig, Germany, SAWzL, and of acatech, the German Academy of Technological Sciences, Germany.
He is currently involved actively in international outreach programs in Europe, Oceania and Pacific Asia, where he was – for example - the Distinguished Senior Visiting Professor at the Tohoku University, Center for Northeast Asian Studies in Sendai, Japan during Spring 2003 and summer 2011; he holds the Distinguished Visiting Chair Professor (2004) position of the National Central University of Taiwan in Chung-Li, Taiwan; the Distinguished Visiting Chair Professor position of *'The Electromagnetics Academy'* of Zhejiang University at Hangzhou in China – involved in the *"advancement of extra-wideband polarimetric imaging radar & SAR theory and technology"*. For his contributions toward linking international research centers of Oceania & East/Austral-Asia via the Americas with Eurasia & Europe, Prof. W-M. Boerner was honored with the distinguished IEEE-GRSS Outstanding Services Award for 2005 and that of IECE-SANE for 2007; and most recently with a Special Recognition on the occasion of the 50th anniversary of IEEE-GRSS during the IGARSS-2012 at Munich, Germany for *"his extraordinary technical contributions to the advancement of radar*

remote sensing and valued services to the Geoscience and Remote Sensing Society of IEEE".

Dr. Boerner is a member of numerous international scientific societies; he is a senior member of the Canadian Association of Physicists (CAP), the American Society for Engineering Education (ASEE), the American and the International Societies for Remote Sensing and Photogrammetry (ASRSP &ISRSP); he is a Life Fellow of IEEE and IEICE; Fellow of the OSA, SPIE, AAAS and of the A.v.H.S. He has been awarded the Alexander von Humboldt U.S. Senior Scientist, the Japan Society for the Promotion of Science Senior U.S. Scientist, and the U.S. Navy Distinguished Senior Professor awards, respectively. He is the University of Illinois Senior Scholar, member of the *Sächsische Akademie der Wissenschaften zu Leipzig*, the *Akademie-Forum (Academy) of Science and Technology of Germany*, and he was awarded the Doctor Honoris Causa of the Tomsk State University Cluster in Tomsk (2000); an Honorary Doctorate, Dr. h.c., from the University of Rennes 1 in Rennes, Brittany, France (2003); and another Honorary Doctorate of Engineering, Dr.-Ing. E-h., from the Friedrich-Alexander University of Erlangen-Nürnberg in Erlangen, Frankonia, Germany (2003). He is a registered engineer with VDE (*Verein Deutscher Ingenieure*), APEM (Association of Professional Engineers of the Province of Manitoba), ISPE &NSPE (Illinois and US National Societies of Professional Engineers); and among others he is a member of the honor societies Sigma Xi, the American and the German Fulbright Associations, and the Alexander von Humboldt Association

Professor Boerner was elected a member of the IUCN SSC/WI Crane Specialist Group 2005-2008, 2009-2012, 2013-2016, and he is an active member of various nature and migratory bird conservation groups including NABU, BUND, ICF, WBI, WBSJ, WBST, and so on; and he specializes on the conservation of wetland and desert habitats for cranes – worldwide.

Sang-Eun Park (S'05-M'07) received the B.S. and M.S. degrees in geophysics and Ph.D. degree in radar remote sensing and geophysics from the Seoul National University, Seoul, Korea, in 2000, 2002, and 2007 respectively. From 2007 to September 2009, he worked at the Radar Polarimetry Remote Sensing Group of the University of Rennes 1, Rennes, France, for a post-doctoral fellow on radar polarimetry. From October 2009 to January 2010, he was a project scientist in the Institute of Photogrammetry and Remote Sensing, Vienna University of Technology, Vienna, Austria. He is currently an Assistant Professor in the Graduate School of Science and Technology at Niigata University, Japan. His research interests include polarimetric SAR classification, forward and inverse modeling of microwave vegetation and surface backscattering, and investigation of multi-source data integration methodology.